Published in final edited form as:
Science. 2021 April 09; 372(6538): 156–165. doi:10.1126/science.abb4542.

Targeting the nucleotide salvage factor DNPH1 sensitizes *BRCA*-deficient cells to PARP inhibitors

Kasper Fugger[1,*], **Ilirjana Bajrami**[1], **Mariana Silva Dos Santos**[1], **Sarah Jane Young**[1], **Simone Kunzelmann**[1], **Geoff Kelly**[2], **Graeme Hewitt**[1], **Harshil Patel**[1], **Robert Goldstone**[1], **Thomas Carell**[3], **Simon J. Boulton**[1], **James MacRae**[1], **Ian A. Taylor**[1], **Stephen C. West**[1,*]

[1]The Francis Crick Institute, 1 Midland Road, London NW1 1AT, U.K.

[2]MRC Biomedical NMR Centre, Francis Crick Institute, London NW1 1AT, U.K.

[3]Faculty of Chemistry and Pharmacy, Ludwig-Maximilians-Universität München Butenandtstr. 5-13, Building F, 81377 Munich, Germany

Abstract

Mutations in the *BRCA1* or *BRCA2* tumor suppressor genes predispose individuals to breast and ovarian cancer. In the clinic, these cancers are treated with inhibitors that target poly[ADP-ribose] polymerase (PARP). We show that inhibition of DNPH1, a protein that eliminates the cytotoxic nucleotide hydroxymethyl-deoxyuridine (hmdU) monophosphate, potentiates the sensitivity of *BRCA*-deficient cells to PARP inhibitors (PARPi). Synthetic lethality was mediated by the action of SMUG1 glycosylase on genomic hmdU, leading to PARP trapping, replication fork collapse, DNA break formation and apoptosis. *BRCA1*-deficient cells that acquired resistance to PARPi were re-sensitized by treatment with hmdU and DNPH1 inhibition. Because genomic hmdU is a key determinant of PARPi sensitivity, targeting DNPH1 provides a promising strategy for the hypersensitization of *BRCA*-deficient cancers to PARPi therapy.

The *BRCA1* and *BRCA2* gene products are required for the repair of DNA doublestrand breaks by homologous recombination (HR) (1, 2), and *BRCA*-defective cells exhibit gross chromosomal rearrangements due to their defects in DNA repair (3). Treatment of *BRCA*-defective cells with PARP inhibitors leads to synthetic lethality (4–6), which is now

[*]Corresponding authors: tel +(44)-203-7962071; stephen.west@crick.ac.uk; kasper.fugger@crick.ac.uk.

Author contributions:
Conceptualization: KF
Methodology: KF, IB, MSDS, IAT
Investigation: KF, IB, MSDS, RG, HP, SJY, SK, IAT, GK, GH
Data curation: KF, IB
Resources: TC
Visualization: KF, IB, SCW
Project administration: KF, SCW
Funding acquisition: SCW
Supervision: SCW, SJB, IAT, JM
Writing - original draft: KF, IB, SCW
Writing – review and editing: KF, SCW

Competing interests: KF and SCW are inventors on patents that pertain to the use of DNPH1 inhibitors and hmdU as a mechanism to sensitize HR-deficient cells to PARPi. SJB is scientific co-founder and VP Science Strategy at Artios Pharma Ltd. The other authors declare no competing interests.

Europe PMC Funders Author Manuscripts

exploited in the clinic for the treatment of breast, ovarian, prostate and pancreatic cancers. PARPi induced cytotoxicity is thought to be caused, at least in part, by the trapping of PARP1 on DNA lesions such as base excision repair (BER) intermediates and genomic ribonucleotides (7, 8). However, despite good initial response, many tumors develop PARPi resistance leading to aggressive tumor growth (9). We therefore sought to identify ways to potentiate PARPi therapy and overcome resistance of HR-deficient cancer cells. To do this, we carried out a genome-wide CRISPR-Cas9 screen using HR-deficient eHAP *MUS81*$^{-/-}$ cells, that are defective in the resolution of recombination intermediates (10). *MUS81*$^{-/-}$ cells were generated by CRISPR genome editing (11) (Fig. S1A) and found to be hypersensitive to the PARPi olaparib, as reported previously (8). Sensitivity was rescued by complementation with wild-type *MUS81* but not a nuclease dead allele (Fig. S1A and B).

CRISPR screen for modulators of PARPi sensitivity

MUS81$^{-/-}$ cells were transduced with the lentiviral-based Brunello genome-wide CRISPR sgRNA library (12), followed by treatment with olaparib for 10 days (Fig. S1C). The LD_{80} dose used allowed us to identify both dropout (sensitizing) and enriched (resistance-causing) gRNAs. Bioinformatic analyses of the gRNA reads using the MAGeCK algorithm identified several determinants of PARPi sensitivity (Fig. 1A and Table S1). PARPi resistance was observed with gRNAs that targeted PARP1 and the de-PARylation factor PARG, which counteracts the cytotoxic effects of PARP trapping (7, 13) or restore PARP activity (14). Sensitizing gRNAs included several base excision repair (BER) factors (Fig. 1A), indicating that defective BER is synthetic lethal with PARPi, likely through increased PARP trapping on repair intermediates. Furthermore, Gene Ontology and STRING protein interaction analyses revealed an enrichment of DNA repair enzymes involved in BER and Fanconi anemia (Fig. S1D and E), as previously observed (15). Inactivation of factors involved in nicotinamide adenine dinucleotide (NADH) metabolism and mitochondrial homeostasis also sensitized cells to PARPi, potentially through the formation of increased reactive oxygen species (ROS) as a result of mitochondrial dysfunction (16), induced DNA damage, and PARP trapping (17).

The highest-ranking hit from the screen was DNPH1/RCL (2′-deoxynucleoside 5′-monophosphate N-glycosidase) (Fig. 1A), a c-Myc target that is overexpressed in various tumors (18, 19). It has been suggested that DNPH1 is involved in nucleotide salvage pathways or as a sanitizer that removes modified or anomalous nucleotides from the nucleotide pool to prevent their incorporation into DNA (20). Disruption of a second nucleotide sanitizer ITPA (inosine triphosphatase), which dephosphorylates dITP to limit its incorporation into DNA (21), also sensitized *MUS81*$^{-/-}$ cells to olaparib. *DNPH1* and *ITPA*, which were also identified in previous PARPi screens (8, 22), were validated as *bona fide* hits using individual CRISPR-generated knock-out (KO) cell lines (Fig. S2A and B). Disruption of either gene in eHAP cells did not impact cell growth or viability, but sensitized HR-deficient *MUS81*$^{-/-}$ cells to treatment with olaparib (Fig. 1B, S2C and S2D). These results indicate that their target nucleotides are a source of endogenous DNA lesions underlying PARPi cytotoxicity.

The marked olaparib sensitivity of the *MUS81*$^{-/-}$ *DNPH1*$^{-/-}$ cells, combined with the uncharacterized biological function of *DNPH1*, led us to focus on the role of this gene in potentiating the effect of PARPi on HR-deficient cells. DNPH1 was found to be expressed in various cell lines including normal epithelial cells (RPE-1 and MCF10A) and the breast tumor-derived *BRCA1-deficient* cancer cell line SUM149 (*BRCA1*^{mut}) (23) (Fig. S2E). Genetic disruption of *DNPH1* in SUM149 *BRCA1*- or DLD1 *BRCA2*-defective cells (Fig. S2F and S2G), resulted in their sensitization to olaparib (Fig. 1C-E and Fig. S2H). This effect was exclusive to PARPi, as little or no sensitization was observed in *DNPH1*-deficient cells exposed to a variety of DNA damaging agents including cisplatin, methyl methanesulfonate (MMS), camptothecin (CPT), ultraviolet (UV) or ionizing irradiation (IR) (Fig. S2I-M). The *BRCA2*$^{-/-}$ *DNPH1*$^{-/-}$ cells exhibited a smaller colony size indicative of decreased growth rate (Fig. 1C). *BRCA2* wild-type (WT) and SUM149 isogenic revertant cells, in which the reading frame of *BRCA1* had reverted to wild-type (23), were insensitive to *DNPH1* loss and olaparib treatment. Taken together, these results show that *DNPH1* inactivation specifically sensitizes clinically relevant *BRCA*-deficient cells to PARPi treatment.

DNPH1 targets hmdUMP to limit genomic incorporation

DNPH1 hydrolyzes deoxyribonucleoside monophosphates (dNMPs) in vitro (20), but its biological nucleotide target(s) and function(s) remain unknown. To determine the precise target of DNPH1, we carried out metabolomic analyses of the nucleoside composition of genomic DNA in wild-type, *DNPH1*$^{-/-}$ and *ITPA*$^{-/-}$ cells. As expected, increased amounts of genomic deoxyinosine (dI) were found in the *ITPA*$^{-/-}$ cells (Fig. S3A), validating our metabolomic approach. In the *DNPH1*$^{-/-}$ cells, however, we observed a specific increase of 5-hydroxymethyl-deoxyuridine (hmdU) in genomic DNA (Fig. 2A). hmdU is a cytotoxic nucleoside arising from either oxidative damage (24) or deamination of 5-hydroxymethyl-deoxycytidine (hmdC) during epigenetic regulation (25). No significant change in other genomic nucleosides was observed (Fig. 2A). Quantification of genomic hmdU showed ~5 per million dN in WT and approximately 15 per million in *DNPH1*$^{-/-}$ cells (Fig. S3B). Because DNPH1 hydrolyses dNMPs, these results suggest that DNPH1 acts upon hmdU monophosphate (hmdUMP) in the nucleotide pool to limit genomic DNA incorporation. In support of this, treatment of *DNPH1*$^{-/-}$ cells with hmdU resulted in a ~10-fold increase in hmdUMP in the nucleotide pool (Fig. 2B), in comparison to a ~3-fold increase in genomic hmdU as compared to WT cells (Fig. S3C). These results show that DNPH1 acts upon hmdUMP to limit its incorporation into DNA.

To determine whether DNPH1 directly hydrolyzes hmdUMP, we purified recombinant human DNPH1, as well as the active site mutant DNPH1^{E104Q} (Fig. 2C). DNPH1, but not DNPH1^{E104Q}, efficiently hydrolyzed hmdUMP to yield hmU nucleobase (shown schematically in Fig. 2D) with a reaction rate of 7.3 ±0.2 min^{-1} (Fig. 2E, S3D and S3E). No detectable activity was observed towards any of the canonical dNMPs (Fig. 2F). The related nucleotides hmdCMP and dUMP were hydrolyzed ~40 and ~110 times slower, respectively (Fig. 2E). To strengthen these findings and directly assess the dNMP preference of DNPH1, we used time-resolved ^{1}H NMR spectroscopy for the simultaneous detection of dNMP hydrolysis, in a mixture that combined hmdUMP with canonical dNMPs in a single reaction.

We found that under these conditions, whilst hmdUMP was fully hydrolyzed after 120 minutes, there was no detectable hydrolysis of any the canonical dNMPs (Fig. 2G and Fig. S3F and S3G). These results confirm that hmdUMP is the direct biological target of DNPH1.

hmdU hypersensitizes HR-deficient cells to PARPi

To determine whether the observed increase in genomic hmdU in *DNPH1*-deficient cells was responsible for the sensitization of HR-deficient cells to PARPi, *MUS81*$^{-/-}$ cells were treated with a panel of deoxynucleosides carrying nucleobases modified by methylation, hydroxylation, deamination, and oxidation, in the presence or absence of olaparib. Co-treatment with hmdU and olaparib induced strong synthetic lethality (Fig. 3A), showing that hmdU potentiates PARPi treatment. hmdU/PARPi treatment also induced synthetic lethality in the SUM149 *BRCA1* mutant cell line (Fig. 3B and S4A and S4B), as well as DLD1 *BRCA2*-defective cells (Fig. 3C and S4C). In contrast, *BRCA* proficient isogenic cell lines were insensitive to the treatment (Fig. 3B and C, S4A-C).

We also observed that hmdC induced synthetic lethality with PARPi (Fig. 3A). To determine whether PARPi potentiation by hmdC was caused by increased hmdU incorporation, we analyzed the genomic nucleotide composition of hmdC-treated cells and found increased amounts of genomic hmdU (Fig. S4D). hmdU was further increased in *DNPH1*$^{-/-}$ cells, indicating that hmdC is converted to hmdU in the nucleotide pool where it is targeted by DNPH1. We did not observe any increase in genomic hmdC, in agreement with previous reports (26). Comparison of genomic hmdU incorporation following exposure of WT cells to hmdU (Fig. S3C) or hmdC nucleosides (Fig. S4D) revealed that hmdC treatment resulted in ~15-fold less hmdU incorporation, in accord with its lower cytotoxicity (Fig. 3A and 3D).

To explore the biological function of DNPH1 in response to aberrant nucleotides, *DNPH1*$^{-/-}$ cells were exposed to a panel of ribonucleosides and deoxyribonucleosides, and cell viability was measured. Strikingly, HR-deficient *MUS81*$^{-/-}$ *DNPH1*$^{-/-}$ double KOs were hypersensitive to treatment with hmdU and to a lesser extent hmdC (Fig. 3D), even in the absence of PARPi. Treatment with their ribonucleoside counterparts hmU or hmC did not affect cell viability (Fig. 3D), demonstrating that the cytotoxic effect requires DNA incorporation. Complementation with wild-type DNPH1, but not the active site mutant DNPH1^{E104A} (20), rescued the cells from hmdU-induced cytotoxicity (Fig. S4E and F).

Because HR-deficient *DNPH1*$^{-/-}$ cells are sensitive to hmdU treatment, we speculated that hmdU treatment could hyper-sensitize these cells to PARPi and found that *BRCA2*$^{-/-}$ *DNPH1*$^{-/-}$ cells were particularly sensitive to PARPi when co-treated with a low dose of hmdU (50 nM). Indeed, ~10 times less PARPi was required to achieve the same level of killing (Fig. 3E). Our results show that synthetic lethality can be induced in a variety of HR-deficient backgrounds and that DNPH1 and its target hmdU may have therapeutic potential.

The cellular origins of hmdU

Nucleotide salvage pathways provide an energy-efficient way to recycle deoxyribonucleosides that arise from the breakdown of DNA or extracellular uptake.

Cytidine nucleotides carrying epigenetic marks such as hmdC are thought to be deaminated to produce the uridine counterpart hmdU (26). To determine whether hmdU arises from hmdC deamination and to identify factors involved in this pathway, we carried out a CRISPR screen in *MUS81*$^{-/-}$ cells exposed to hmdC. Bioinformatic analysis revealed that the loss of factors involved in nucleoside phosphorylation such as deoxycytidine kinase (DCK) and thymidylate kinase (DTYMK) rendered cells resistant to hmdC treatment (Fig. 4A). The screen also showed that loss of *DNPH1* sensitized cells to hmdC, confirming the critical role that DNPH1 plays in the survival of HR-deficient cells by eliminating hmdUMP.

The loss of the gene encoding dCMP deaminase, DCTD, rendered eHAP cells resistant to hmdC (Fig. 4A), indicating that DCTD deaminates hmdC monophosphate (hmdCMP) to produce hmdUMP in the nucleotide pool. Loss of *DCTD* also conferred resistance to olaparib (Fig. 1A), presumably as a consequence of decreased genomic hmdU incorporation. To test this possibility, we generated *DCTD*$^{-/-}$ cell lines in the *MUS81*-deficient background (Fig. S4G) and found that they were resistant to co-treatment with olaparib and hmdC, but not hmdU (Fig. S4H). The increased sensitization of *MUS81*$^{-/-}$ cells to olaparib upon *DNPH1* ablation was reversed by codisruption of *DCTD* (Fig. 4B), showing that the synthetic lethality results from DCTD-mediated formation of hmdUMP. Consistent with these results, the increase in genomic hmdU observed in *DNPH1*$^{-/-}$ cells was also reversed by disruption of *DCTD* (Fig. 4C).

Because cytidine deaminase (CDA) targets dNs and DCTD targets dNMPs, we next determined whether the deamination of hmdC to hmdU occurs at the nucleoside or nucleoside monophosphate level. To do this, we generated *CDA*$^{-/-}$ and *DCTD*$^{-/-}$ cell lines (Fig. S4I). We found that loss of *DCTD*, but not *CDA*, completely abolished hmdC-mediated deamination and hmdU incorporation (Fig. 4D), showing that hmdCMP deamination in eHAP cells occurs at the dNMP level, similar to hmdUMP hydrolysis by DNPH1.

During epigenetic regulation, genomic hmdC is produced by dioxygenase-mediated hydroxylation of methylated cytosine by the Ten Eleven Translocation (TET) enzymes (27). To determine whether breakdown and subsequent deamination of hmdC-containing genomic DNA was responsible for the increased sensitivity of *DNPH1* deficient cells to PARPi, cells were depleted of *TET1* and *TET2* using CRISPR-Cas9 (Fig. S4J). Loss of TET1 and TET2 partially reversed PARPi sensitivity in *MUS81*$^{-/-}$ *DNPH1*$^{-/-}$ cells (Fig. 4E). Furthermore, the *TET1/TET2* depleted cells were sensitive to hmdU/olaparib (Fig. 4E) indicating that the observed rescue was not due to a general resistance of TET-deficient cells to the cytotoxic effects of hmdU. Moreover, these data support the hypothesis that hmdUMP, produced by DCTD-dependent deamination of hmdCMP, is the biological target of DNPH1, thereby constituting a metabolic pathway that disposes of epigenetically modified nucleotides (shown schematically in Fig. 4F).

SMUG1 mediates synthetic lethality through PARP trapping

Our screens further revealed that loss of single-strand-selective monofunctional uracil-DNA glycosylase 1 (SMUG1) caused resistance to olaparib or hmdC treatment in HR-defective

cells (Fig. 1A and 4A). Since SMUG1 is the primary glycosylase responsible for removing hmdU from genomic DNA (28), we speculated that the action of SMUG1 on hmdU drives synthetic lethality. To test this, we generated *SMUG1*$^{-/-}$ cells (Fig. S5A) and found that whilst *MUS81*$^{-/-}$ cells were hypersensitive to hmdU/olaparib treatment, *MUS81*$^{-/-}$ *SMUG1*$^{-/-}$ cells were completely resistant (Fig. 5A). Similar observations were made in DLD1 *BRCA2*-deficient cells following *SMUG1* disruption (Fig. S5B). Furthermore, the increased PARPi sensitivity observed in *DNPH1*$^{-/-}$ *BRCA2*$^{-/-}$ cells was reversed by loss of *SMUG1* (Fig. S5C). Complementation of the *MUS81*$^{-/-}$ *SMUG1*$^{-/-}$ cells with wild-type SMUG1, but not catalytically inactive SMUG1^{G87Y}, restored cell death upon hmdU/olaparib treatment (Fig. S5D and E). Taken together, these results show that SMUG1-dependent excision of genomic hmdU is the underlying basis for the synthetic lethality.

PARPi-induced synthetic lethality is caused, at least in part, by PARP trapping, whereby PARP proteins are trapped on various DNA structures including single-strand breaks (SSBs) and BER intermediates (7). Consequently, and as also confirmed by our screen (Fig. 1A), loss of PARP1 causes PARPi resistance, by alleviating the dominant-negative effect of PARP trapping (7, 13). We therefore analyzed PARP trapping in cells exposed to hmdU/olaparib and found increased chromatin association of PARP1 in comparison with olaparib treatment alone (Fig. 5B). Additionally, we observed the induction of DNA damage checkpoint signaling (γH2AX phosphorylation) and apoptosis (PARP1 cleavage). Ablation of *SMUG1* fully reversed these hmdU/olaparib-induced phenotypes (Fig. 5B), showing that PARP trapping occurs on BER intermediates that arise from SMUG1-mediated hmdU excision. In contrast, we did not observe any difference in PARP trapping or DNA damage signaling between WT and *SMUG1*-deficient cells treated with the alkylating agent MMS (Fig. 5B), confirming that the lack of PARP trapping in *SMUG1*-deficient cells was not due to a general BER defect. Consistent with the hypothesis that PARP trapping was responsible for increased cell killing in *DNPH1*-defective cells following PARPi, we found that olaparib sensitivity in *DNPH1*$^{-/-}$ cells was PARP1-dependent (Fig. 5C and Fig. S5F). Similar results were observed with other PARPi such as veliparib (Fig. S5G) and talazoparib (Fig. S5H). These results show that PARP trapping occurs in a hmdU- and SMUG1-dependent manner following PARPi treatment.

To understand the hmdU/SMUG1-induced mechanism of cell death, DNA double strand break (DSB) formation and DNA damage checkpoint signaling were analyzed in the DLD1 isogenic cell line models. Untreated *BRCA2*$^{-/-}$ *DNPH1*$^{-/-}$ cells showed an increase in checkpoint signaling and replication stress, as evidenced by immunoblotting of phosphorylated H2A histone family member X (γH2AX), phosphorylated KRAB-associated protein-1 (pKAP1), or Checkpoint kinase 1 (pCHK1), and PARP1 cleavage (apoptosis) (Fig. 5D, and S5I). In addition, low amounts of small molecular weight DNA were observed as smears by PFGE, indicative of apoptosis (Fig. 5D). Taken together with the slight growth defect observed in *BRCA2*$^{-/-}$ *DNPH1*$^{-/-}$, as compared to *BRCA2*$^{-/-}$ cells (Fig. 1C), these results indicate that DNPH1 loss causes endogenous DNA damage because of replication stress.

Following exposure to hmdU or hmdU/olaparib, but not olaparib alone, we observed a large increase in DSB formation, increased amounts of γH2AX, pKAP1, and pCHK1, and PARP1

cleavage in the *BRCA2*$^{-/-}$ *DNPH1*$^{-/-}$ cells (Fig. 5D, S5J, S6A and S6B). Upon co-treatment with a caspase inhibitor (Z-VAD-FMK), we observed increased DSB formation and a reduction in the low molecular weight smears (Fig. S6C), consistent with apoptosis occurring from elevated DSB formation in *BRCA2*$^{-/-}$ *DNPH1*$^{-/-}$ cells. All phenotypes were reversed by disruption of *SMUG1*, demonstrating that SMUG1-induced DSB formation is the underlying cause of PARPi-induced synthetic lethality brought about by PARP trapping at sites of hmdU excision.

Excision of aberrant bases by DNA glycosylases leads to the formation of abasic sites that interfere with replication fork progression (29). We therefore explored the possibility that synthetic lethality results from replication fork collapse at hmdU-induced abasic sites. We found that hmdU/olaparib treatment of the *DNPH1*$^{-/-}$ cells led to increased RAD51 foci, which were suppressed by loss of *BRCA2* (Fig. 5E and S6D), indicative of HR-mediated DSB repair. We next analyzed replication fork progression by measuring the symmetry of bidirectional forks (Fig. 5F). Whereas forks from untreated cell lines were largely indistinguishable from each other (Fig. S6E and S6F), an increase in asymmetric forks was observed in *BRCA2*$^{-/-}$ *DNPH1*$^{-/-}$ cells upon hmdU/olaparib treatment, as compared with *BRCA2*$^{-/-}$ cells (Fig. 5G and H). These results indicate that the observed DSBs are a consequence of replication fork collapse. Consistent with this, fork asymmetry induced by hmdU/olaparib was suppressed by loss of SMUG1.

Killing of PARPi-resistant *BRCA1*-deficient cells

PARPi resistance arises by: (i) reversion of the *BRCA* genes to wild-type (9), (ii) loss or mutation of *PARP1* (7, 13) or *PARG* (14), or (iii) in the case of *BRCA1*-deficient cells, by restoration of HR-proficiency through inactivation of the p53-binding protein 1 (53BP1)-SHIELDIN pathway (9, 30). We have shown that *BRCA*-deficient cells can be efficiently killed by either potentiating PARPi by hmdU or in a PARPi-independent manner by hmdU treatment upon *DNPH1* ablation. To determine whether these treatment strategies re-sensitize PARPi-resistant *BRCA1*-deficient cells, we compared their effects in *BRCA1* mutant, wild-type SUM149, or PARPi-resistant cell lines depleted of 53BP1, SHLD1, or PARP1 using lentiCRISPR (Fig. S7A and B). Compared with olaparib alone, we found that co-treatment with hmdU/olaparib led to a ~3-fold expansion of the therapeutic window (Fig. 6A, left and right panels). hmdU treatment efficiently re-sensitized PARPi-resistant *BRCA1*^{mut} cells depleted of *53BP1, SHLD1* (Fig. 6B and S7C, left and right panels), or to a lesser extent *PARP1* (Fig. 6C, left and right panels), to olaparib treatment.

While ablation of *DNPH1* in *BRCA1*-deficient cells, or treatment with hmdU alone, had only mild effects on cell viability, hmdU selectively killed the *BRCA1*^{mut} *DNPH1*$^{-/-}$ cells (Fig. 6A, center and right panels). PARPi-resistant *BRCA1*^{mut} *DNPH1*$^{-/-}$ cell lines depleted of *53BP1* (Fig. 6B, center panel), *SHLD1* (Fig. S7C, center panel) or *PARP1* (Fig. 6C, center panel), were efficiently killed by hmdU treatment. Indeed, the therapeutic windows increased ~10 to 20-fold compared to olaparib alone (Fig. 6B and C, right panels, and S7C, right panel). There was no significant effect on the sensitivity of HR-proficient *DNPH1*$^{-/-}$ cells depleted of *53BP1* or *PARP1* to olaparib or hmdU treatment, compared to *DNPH1*$^{-/-}$

cells (Fig. S7D and E), indicating that 53BP1 or PARP1 alone were not required for the repair of DSBs resulting from hmdU lesions.

To determine whether chemical inhibition of DNPH1 could also sensitize cells to hmdU, we used the DNPH1 competitive inhibitor, N^6-benzyladenosine (DNPH1i) (31), that limits the activity of DNPH1 in vitro (Fig. 6D). While treatment of *MUS81*-deficient cells with DNPH1i or hmdU alone had a mild effect on cell viability, co-treatment with hmdU/DNPH1i selectively killed the HR-deficient cells (Fig. S7F). This concentration of DNPH1i did not further sensitize *MUS81*$^{-/-}$ *DNPH1*$^{-/-}$ cells to hmdU, confirming its specificity (Fig. S7G). Similarly, hmdU/DNPH1i treatment killed *BRCA1*-defective cells (Fig. 6E), as well as PARPi-resistant *BRCA1*-mutant cell lines depleted of *PARP1* (Fig. 6F) or *53BP1* (Fig. S7H). These results provide proof of concept that DNPH1 inhibition can be used to sensitize *BRCA*-deficient cells to PARPi or hmdU treatment. DNPH1i treatment did not decrease the viability of *BRCA1*^{mut} *DNPH1*$^{-/-}$ cells treated with hmdU, demonstrating on-target effects of the drug (Fig. S7I).

Discussion

Rapidly proliferating cancer cells are dependent on a steady supply of nucleotides which is achieved by *de novo* synthesis and salvage pathways that are upregulated in many cancers. However, the re-incorporation of recycled nucleotides carrying epigenetic marks is undesirable due to their potential to alter gene expression, and they are therefore excluded from DNA incorporation by the selectivity of nucleotide kinases (26). How cells deal with these modified nucleotides is largely unknown. Here we define a metabolic pathway whereby cells eliminate epigenetically modified hmdCMP, in a two-step process entailing deamination to cytotoxic hmdUMP by DCTD, followed by DNPH1-mediated hydrolysis into hmU and dRP (Fig. 4F). Our results indicate that hmdC(MP) originates in part from the breakdown of TET hydroxymethylated DNA. Indeed, exonucleolytic processing which occurs during DNA repair yields nucleoside monophosphates such as hmdCMP, which is the level at which both DCTD and DNPH1 operate, thereby constituting a linear pathway for disposal of hmdCMP. In addition to DNA metabolism, other sources of salvaged nucleotides include extracellular uptake, which is also targeted by the DCTD/DNPH1 pathway to dispose of exogenous hmdU and hmdC nucleosides.

Although we found that genomic hmdU in our cell models predominantly arises through deamination of hmdCMP by DCTD rather than CDA, it is likely that the increased formation of hmdU observed in breast and pancreatic cancer cells with high levels of CDA (26) might result from a gain-of-function activity. Consistent with this, high DCTD expression has been shown to correlate with poor prognosis in patients with malignant glioma (32). We therefore speculate that cancers with high levels of hmdC and/or expression of CDA or DCTD may depend on DNPH1 for survival due to increased levels of cytotoxic hmdUMP. As *DNPH1* is a c-Myc targeted gene, its expression is directly linked to activation of the nucleotide salvage pathway (33), and as such could help cancer cells cope with increased nucleotide metabolism and hmdUMP levels.

Our work demonstrates that the underlying mechanism of PARPi induced synthetic lethality of HR-deficient cells following exposure to hmdU is widespread replication fork collapse, DSB formation and apoptotic cell death (Fig. S8). These events are dependent on SMUG1-mediated PARP trapping. In addition to DNPH1 ablation, we found that loss of ITPA also sensitized cells to PARPi, presumably through increased genomic dI, suggesting that other types of aberrant nucleotides might also lead to PARP trapping and contribute to synthetic lethality. In addition to PARP trapping at BER intermediates (7, 8), several hypotheses have been proposed as causes of synthetic lethality such as excessive fork speed (34), persistent single-strand breaks at unligated Okazaki fragments (35) and/or the formation of replication-associated ssDNA gaps (36). Our present work does not exclude these possibilities as intermediary steps during replication fork collapse.

In summary, we have shown that hmdU is an endogenous DNA lesion that potentiates the response to PARPi therapy. Furthermore, we discovered that PARPi-resistant *BRCA1*-defective cells with loss of either PARP1 or the 53BP1-SHIELDIN pathway, were effectively killed by hmdU (by genetic or chemical ablation of DNPH1) to a similar extent as the non-resistant *BRCA1*-defective cells. As loss of the 53BP1-SHIELDIN pathway restores HR-proficiency through reactivation of DNA end resection (30, 37), our data indicate that BRCA1's role in mediating replication fork protection, rather than HR, is a key event in safeguarding against hmdU/DNPH1i-induced cell death (38, 39). The striking effect of DNPH1 inhibition on the sensitization of *BRCA*-deficient cancer cells to PARPi and hmdU treatment indicates that DNPH1 should be investigated as a potential druggable target.

Supplementary Material

Refer to Web version on PubMed Central for supplementary material.

Acknowledgments

We thank members of the West lab for their help and encouragement, the Francis Crick Institute's Advanced Sequencing, Peptide Chemistry, Equipment Park and High Throughput Screening STPs, Mark O'Connor and Josep Forment (AstraZeneca) for help and insightful comments, Christopher Lord (ICR, London) for providing cell lines, Pierre-Alexandre Kaminski (Institute Pasteur, Paris) for the DNPH1 bacterial expression plasmids and Jesper Christensen (BRIC, Copenhagen) for TET1 antibody.

Funding

This work was supported by:

The Francis Crick Institute grant FC0010212 (SCW). The Francis Crick Institute receives core funding from Cancer Research UK, the Medical Research Council, and the Wellcome Trust.

The European Research Council grant ERC-ADG-666400 (SCW)

The Louis-Jeantet Foundation (SCW)

The Benzon Foundation (KF)

The Lundbeck Foundation (KF)

As this research was funded in part by the Wellcome Trust, for the purpose of Open Access, the article is published with a CC BY public copyright licence.

Europe PMC Funders Author Manuscripts

Data and materials availability

All cell lines and reagents will be provided on request. Data are available in the manuscript and supplementary materials.

References and notes

1. Moynahan ME, Chiu JW, Koller BH, Jasin M. BRCA1 controls homology-directed DNA repair. Mol Cell. 1999; 4:511–518. [PubMed: 10549283]
2. Moynahan ME, Pierce AJ, Jasin M. BRCA2 is required for homology-directed repair of chromosomal breaks. Mol Cell. 2001; 7:263–272. [PubMed: 11239455]
3. Ewald IP, et al. Genomic rearrangements in BRCA1 and BRCA2: A literature review. Genet Mol Biol. 2009; 32:437–446. [PubMed: 21637503]
4. Bryant HE, et al. Specific killing of BRCA2-deficient tumours with inhibitors of poly(ADP-ribose) polymerase. Nature. 2005; 434:913–917. [PubMed: 15829966]
5. Farmer H, et al. Targeting the DNA repair defect in BRCA mutant cells as a therapeutic strategy. Nature. 2005; 434:917–921. [PubMed: 15829967]
6. Pommier Y, O'Connor MJ, de Bono J. Laying a trap to kill cancer cells: PARP inhibitors and their mechanisms of action. Sci Transl Med. 2016; 8362ps317
7. Murai J, et al. Trapping of PARP1 and PARP2 by clinical PARP inhibitors. Cancer Res. 2012; 72:5588–5599. [PubMed: 23118055]
8. Zimmermann M, et al. CRISPR screens identify genomic ribonucleotides as a source of PARP-trapping lesions. Nature. 2018; 559:285–289. [PubMed: 29973717]
9. Noordermeer SM, van Attikum H. PARP inhibitor resistance: A tug-of-war in BRCA-mutated cells. Trends Cell Biol. 2019; 29:820–834. [PubMed: 31421928]
10. Wyatt HDM, Sarbajna S, Matos J, West SC. Coordinated actions of SLX1-SLX4 and MUS81-EME1 for Holliday junction resolution in human cells. Mol Cell. 2013; 52:234–247. [PubMed: 24076221]
11. Ran FA, et al. Genome engineering using the CRISPR-Cas9 system. Nat Protoc. 2013; 8:2281–2308. [PubMed: 24157548]
12. Doench JG, et al. Optimized sgRNA design to maximize activity and minimize off-target effects of CRISPR-Cas9. Nat Biotechnol. 2016; 34:184–191. [PubMed: 26780180]
13. Pettitt SJ, et al. Genome-wide and high-density CRISPR-Cas9 screens identify point mutations in PARP1 causing PARP inhibitor resistance. Nat Commun. 2018; 9:1849. [PubMed: 29748565]
14. Gogola E, et al. Selective loss of PARG restores PARylation and counteracts PARP inhibitor-mediated synthetic lethality. Cancer Cell. 2018; 33:1078–1093. [PubMed: 29894693]
15. Mengwasser KE, et al. Genetic screens reveal FEN1 and APEX2 as BRCA2 synthetic lethal targets. Mol Cell. 2019; 73:885–899. [PubMed: 30686591]
16. Zorov DB, Juhaszova M, Sollott SJ. Mitochondrial reactive oxygen species (ROS) and ROS-induced ROS release. Physiol Revs. 2014; 94:909–950. [PubMed: 24987008]
17. Luo X, Kraus WL. On PAR with PARP: cellular stress signaling through poly(ADP-ribose) and PARP-1. Genes Dev. 2012; 26:417–432. [PubMed: 22391446]
18. Shin S, Bosc DG, Ingle JN, Spelsberg TC, Janknecht R. RCL is a novel ETV/ER81 target gene upregulated in breast tumors. J Cell Biochem. 2008; 105:866–874. [PubMed: 18726892]
19. Lewis BC, et al. Tumor induction by the c-Myc target genes RCL and lactate dehydrogenase A. Canc Res. 2000; 60:6178–6183.
20. Ghiorghi YK, Zeller KI, Dang CV, Kaminski PA. The c-Myc target gene RCL (C6orf108) encodes a novel enzyme, deoxynucleoside 5'-monophosphate N-glycosidase. J Biol Chem. 2007; 282:8150–8156. [PubMed: 17234634]
21. Lin S, et al. Cloning, expression, and characterization of a human inosine triphosphate pyrophosphatase encoded by the ITPA gene. J Biol Chem. 2001; 276:18695–18701. [PubMed: 11278832]

22. DeWeirdt PC, et al. Genetic screens in isogenic mammalian cell lines without single cell cloning. Nat Commun. 2020; 11:752. [PubMed: 32029722]
23. Drean A, et al. Modeling therapy resistance in BRCA1/2-mutant cancers. Mol Cancer Ther. 2017; 16:2022–2034. [PubMed: 28619759]
24. Yu Y, Cui Y, Niedernhofer LJ, Wang Y. Occurrence, biological consequences, and human health relevance of oxidative stress-induced DNA damage. Chem Res Toxicol. 2016; 29:2008–2039. [PubMed: 27989142]
25. Guo JU, Su Y, Zhong C, Ming G, Song H. Hydroxylation of 5-methylcytosine by TET1 promotes active DNA demethylation in the adult brain. Cell. 2011; 145:423–434. [PubMed: 21496894]
26. Zauri M, et al. CDA directs metabolism of epigenetic nucleosides revealing a therapeutic window in cancer. Nature. 2015; 524:114–118. [PubMed: 26200337]
27. Yin X, Xu Y. Structure and function of TET enzymes. Adv Exp Med Biol. 2016; 945:275–302. [PubMed: 27826843]
28. Masaoka A, et al. Mammalian 5-formyluracil-DNA glycosylase. 2. Role of SMUG1 uracil-DNA glycosylase in repair of 5-formyluracil and other oxidized and deaminated base lesions. Biochemistry. 2003; 42:5003–5012. [PubMed: 12718543]
29. Kunz C, et al. Base excision by thymine DNA glycosylase mediates DNA-directed cytotoxicity of 5-fluorouracil. PLoS Biol. 2009; 7e91 [PubMed: 19402749]
30. Jaspers JE, et al. Loss of 53BP1 causes PARP inhibitor resistance in BRCA1-mutated mouse mammary tumors. Cancer Discov. 2013; 3:68–81. [PubMed: 23103855]
31. Amiable C, Pochet S, Padilla A, Labesse G, Kaminski PA. N6-substituted AMPs inhibit mammalian deoxynucleotide N-hydrolase DNPH1. PLoS One. 2013; 8e80755 [PubMed: 24260472]
32. Hu Z, et al. Gene expression and methylation analyses suggest DCTD as a prognostic factor in malignant glioma. Sci Rep. 2017; 711568 [PubMed: 28912488]
33. Cunningham JT, Moreno MV, Lodi A, Ronen SM, Ruggero D. Protein and nucleotide biosynthesis are coupled by a single rate-limiting enzyme, PRPS2, to drive cancer. Cell. 2014; 157:1088–1103. [PubMed: 24855946]
34. Maya-Mendoza A, et al. High speed of fork progression induces DNA replication stress and genomic instability. Nature. 2018; 559:279–284. [PubMed: 29950726]
35. Hanzlikova H, et al. The importance of poly(ADP-ribose) polymerase as a sensor of unligated Okazaki fragments during DNA replication. Mol Cell. 2018; 71:319–333. [PubMed: 29983321]
36. Cong K, et al. PARPi synthetic lethality derives from replication-associated single-stranded gaps. bioRxiv. 2019; doi: 10.1101/781989
37. Bunting SF, et al. 53BP1 inhibits homologous recombination in *BRCA1*-deficient cells by blocking resection of DNA breaks. Cell. 2010; 141:243–254. [PubMed: 20362325]
38. Daza-Martin M, et al. Isomerization of BRCA1-BARD1 promotes replication fork protection. Nature. 2019; 571:521–527. DOI: 10.1038/s41586-019-1363-4 [PubMed: 31270457]
39. Bhat KP, Cortez D. RPA and RAD51: fork reversal, fork protection, and genome stability. Nat Struct Mol Biol. 2018; 25:446–453. [PubMed: 29807999]
40. Essletzbichler P, et al. Megabase-scale deletion using CRISPR/Cas9 to generate a fully haploid human cell line. Genome Res. 2014; 24:2059–2065. [PubMed: 25373145]
41. Sanjana NE, Shalem O, Zhang F. Improved vectors and genome-wide libraries for CRISPR screening. Nat Methods. 2014; 11:783–784. [PubMed: 25075903]
42. Li H, D'urbin RA, G. Fast and accurate short read alignment with Burrows_Wheeler transform. Bioinformatics. 2009; 25:1754–1760. [PubMed: 19451168]
43. Li W, et al. MAGeCK enables robust identification of essential genes from genome-scale CRISPR-Cas9 knockout screens. Genome Biol. 2014; 15:554. [PubMed: 25476604]
44. Traube FR, et al. Isotope-dilution mass spectrometry for exact quantification of noncanonical DNA nucleosides. Nat Protoc. 2019; 14:283–312. [PubMed: 30559375]
45. Chan YW, Fugger K, West SC. Unresolved recombination intermediates lead to a novel class of ultra-fine bridges, chromosome breaks and aberrations. Nat Cell Biol. 2018; 20:92–103. [PubMed: 29255170]

46. Fugger K, et al. FBH1 co-operates with MUS81 in inducing DNA double-strand breaks and cell death following replication stress. Nat Commun. 2013; 4:1423. [PubMed: 23361013]
47. Williams K, et al. TET1 and hydroxymethylcytosine in transcription and DNA methylation fidelity. Nature. 2011; 473:343–348. [PubMed: 21490601]
48. Mi H, Muruganujan A, Thomas PD. PANTHER in 2013: Modeling the evolution of gene function, and other gene attributes, in the context of phylogenetic trees. Nucleic Acids Res. 2013; 41:D377–386. [PubMed: 23193289]
49. Benjamini Y, Kreiger AM, Yeketieli D. Adaptive linear set-up procedures that control the false discovery rate. Genome Res. 2006; 13:491–507.

Europe PMC Funders Author Manuscripts

Europe PMC Funders Author Manuscripts

One sentence summary

Inhibition of the nucleotide sanitizer DNPH1 sensitizes BRCA-deficient cells to treatment with PARP inhibitors.

Europe PMC Funders Author Manuscripts

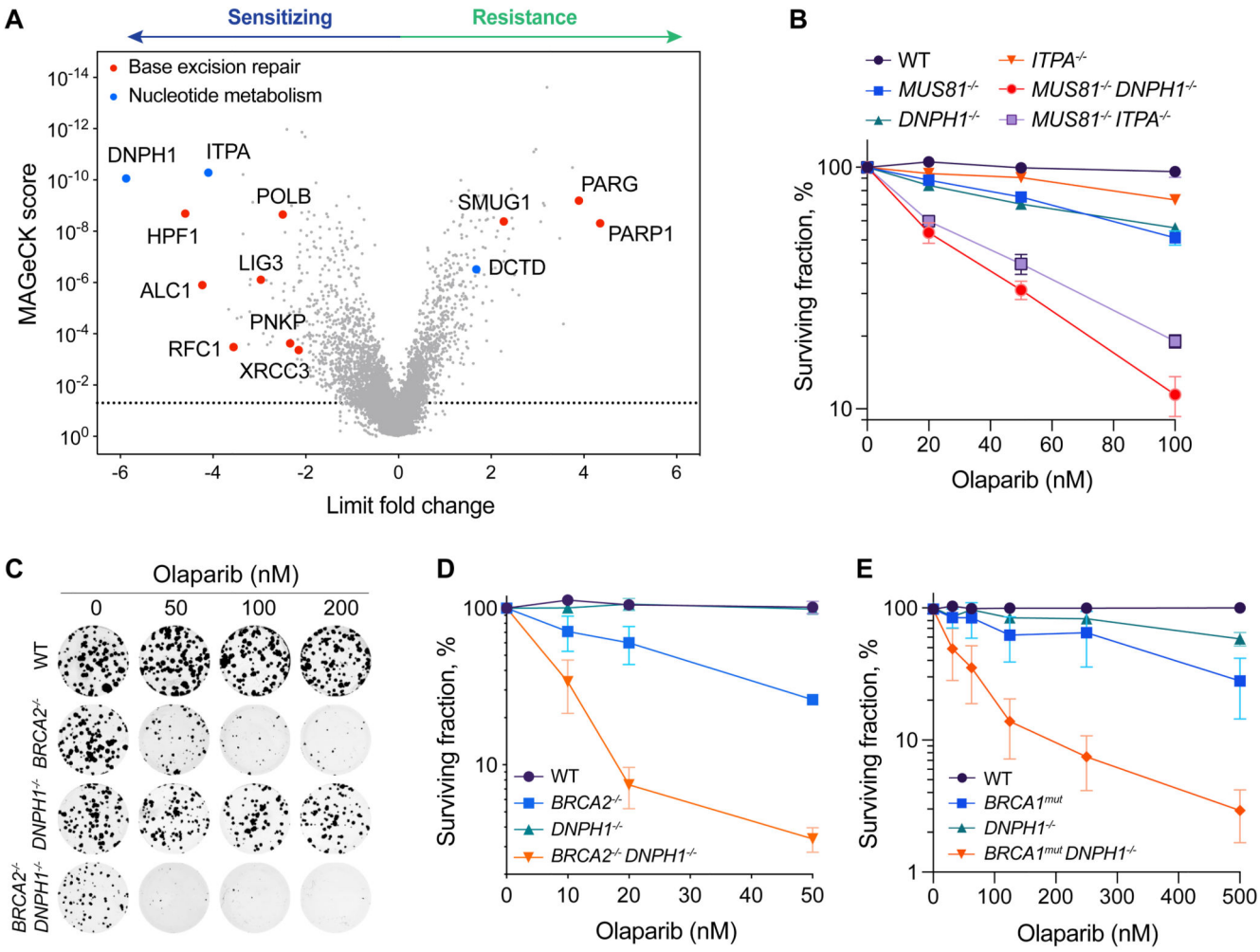

Fig. 1. Loss of DNPH1 sensitizes HR-deficient cells to PARP inhibitors.

(A) Volcano plot showing sgRNA scores from MAGeCK analysis of a genomewide CRISPR-Cas9 dropout/enrichment screen in eHAP *MUS81*$^{-/-}$ cells (olaparib vs mock). Each point represents limit fold change (sensitizing sgRNAs to the left and resistance to the right) with corresponding MAGeCK score. BER and nucleotide metabolism factors are highlighted.

(B) eHAP WT or KO cell lines were treated for 6 days with the indicated doses of olaparib, and viability was determined using CellTiter-Glo (mean with s.e.m; n=3). Data were analyzed using ANOVA for multiple comparisons. *MUS81*$^{-/-}$ vs *MUS81*$^{-/-}$ *DNPH1*$^{-/-}$, p = 0.0013; *MUS81*$^{-/-}$ vs *MUS81*$^{-/-}$ *ITPA*$^{-/-}$, p = 0.0144.

(C) DLD1 WT or KO cell lines were seeded for colony formation and treated continuously for 10 days with olaparib. Colonies were fixed and stained with crystal violet. Well diameter is 22 mm.

(D) DLD1 WT or KO cell lines were treated continuously for 10 days with olaparib. Cell viability was determined, and data analyzed as in (B). *BRCA2*$^{-/-}$ vs *BRCA2*$^{-/-}$ *DNPH1*$^{-/-}$, p < 0.0001.

(E) SUM149 WT (revertant) or KO cell lines were treated for 10 days with olaparib. Cell viability was determined, and data analyzed as in (B). *BRCA1*^{mut} vs *BRCA1*^{mut} *DNPH1* $^{-/-}$, $p = 0.0021$.

Europe PMC Funders Author Manuscripts

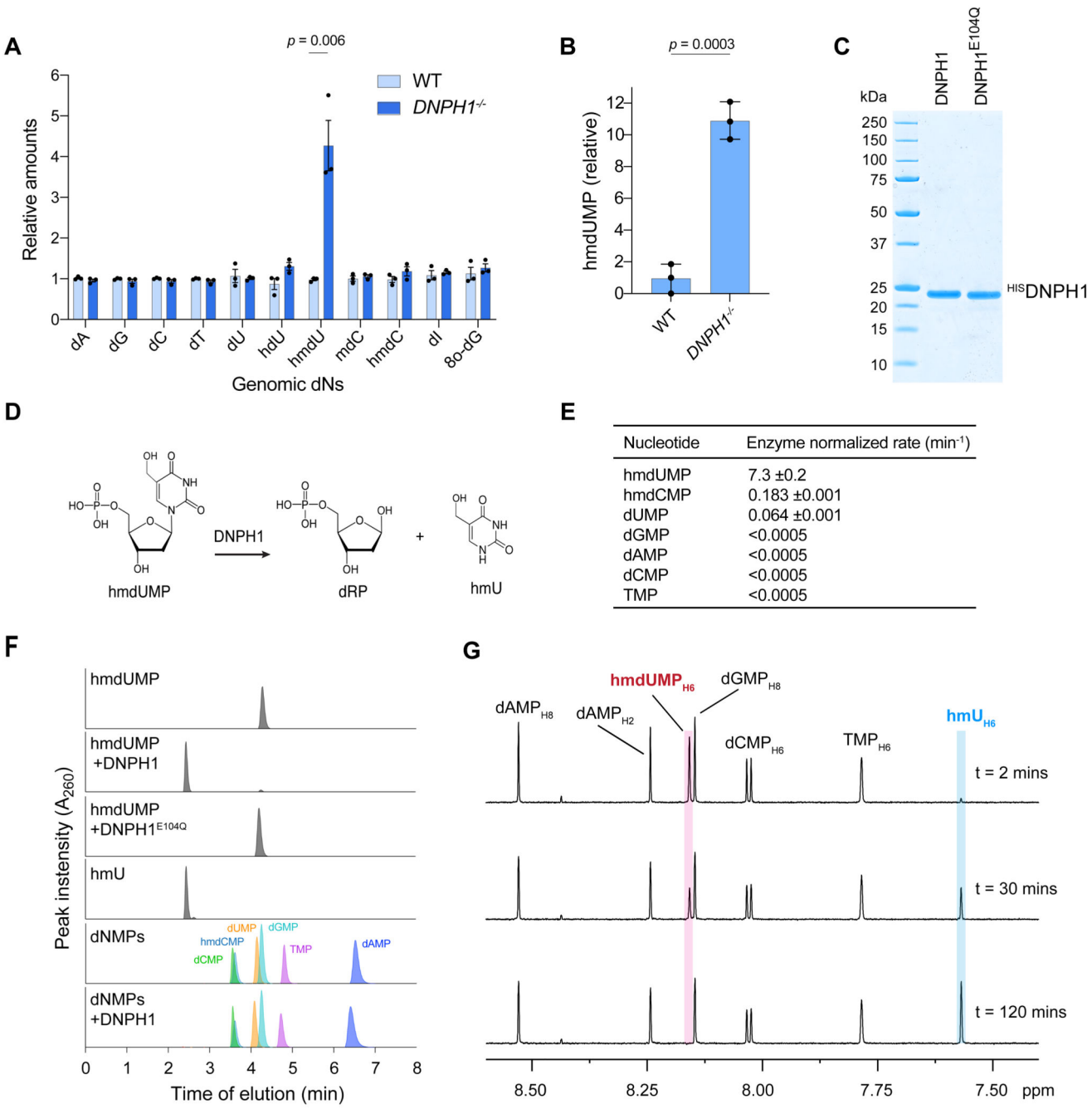

Fig. 2. DNPH1 is a nucleotide sanitizer that hydrolyses hmdUMP to prevent genomic DNA incorporation.

(A) Genomic DNA was extracted from eHAP WT or *DNPH1*$^{-/-}$ cells, digested, and analyzed for its nucleoside composition by LC-MS. The graph depicts the ratio of the indicated nucleosides in *DNPH1*$^{-/-}$ vs WT genomic DNA (mean with s.e.m; n=3).

(B) Nucleotide pools were extracted from eHAP WT or *DNPH1*$^{-/-}$ cells treated with 0.5 μM hmdU for 4 h and analyzed for hmdUMP by LC-MS.

Europe PMC Funders Author Manuscripts

(C) SDS-PAGE of purified HIS-tagged DNPH1 and catalytic site mutant DNPH1^{E104Q} visualized by Instant Blue stain.

(D) Schematic indicating the hydrolysis of hmdUMP by DNPH1 to form deoxyribose phosphate (dRP) and hydroxymethyl uracil (hmU).

(E) Rates of dNMP hydrolysis by DNPH1 were determined by linear regression of data from Figure S3E. Each dNMP was analyzed independently.

(F) Analysis of DNPH1 activity with deoxynucleoside monophosphates (dNMPs). DNPH1 or DNPH1^{E104Q} (4 μM) were incubated individually with the indicated substrates (1 mM) for 45 min. Products were analyzed by RP-HPLC and visualized as chromatograms. Untreated dNMPs and the nucleobase hmU are indicated.

(G) ^{1}H NMR time-resolved spectroscopy of an equimolar mixture of dAMP, dCMP, dGMP, TMP and hmdUMP (0.5 mM each) following incubation with 1 μM DNPH1 for the indicated times. Time-dependent disappearance of hmdUMP (red box) and appearance of hydroxymethyl uracil are highlighted (blue box). The resonances of non-labile base protons from each nucleotide are shown.

Europe PMC Funders Author Manuscripts

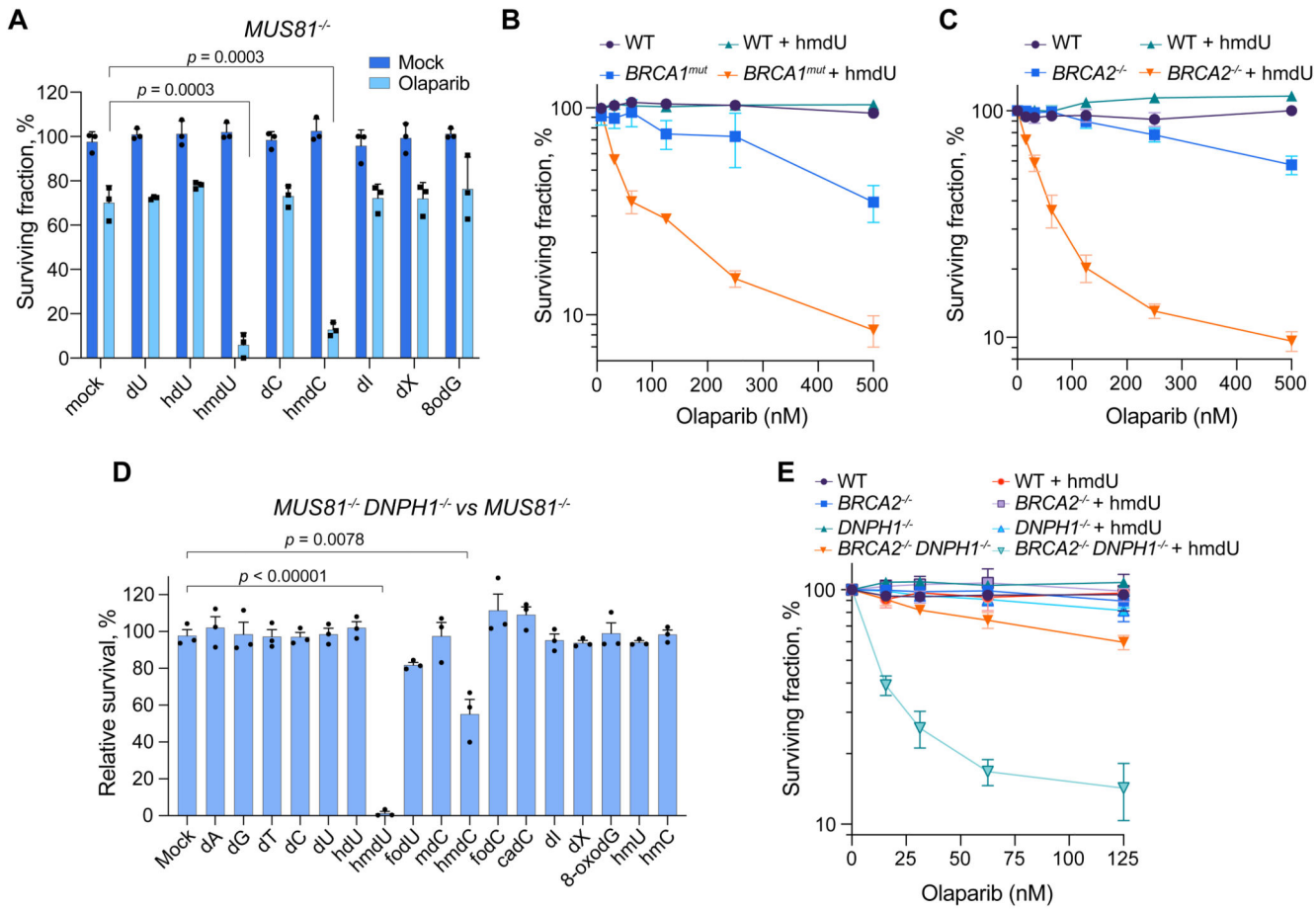

Fig. 3. Sensitization of HR-deficient cells to PARPi by hmdU.

(A) eHAP *MUS81*$^{-/-}$ cells were either untreated or treated with the indicated nucleosides (200 nM) in the presence or absence of olaparib (25 nM) for 6 days. Cell viability was determined using CellTiter-Glo (mean with s.e.m; n=3).

(B) Patient-derived SUM149 *BRCA1*^{mut} (parental) and revertant (WT) cells were treated for 8 days with olaparib in the presence or absence of hmdU (1 μM). Cell viability was determined using CellTiter-Glo. *BRCA1*^{mut} vs *BRCA1*^{mut} + hmdU, $p = 0.0004$.

(C) DLD1 WT and *BRCA2* $^{-/-}$ cells were treated for 10 days with olaparib in the presence or absence of hmdU (1 μM). Cell viability was determined as in (B) *BRCA2*$^{-/-}$ vs *BRCA2*$^{-/-}$ + hmdU, $p < 0.0001$.

(D) eHAP *MUS81*$^{-/-}$ and *MUS81*$^{-/-}$ *DNPH1*$^{-/-}$ cells were either left untreated or treated with the indicated nucleosides (200 nM) for 6 days. Cell viability was determined as in (A). Bar chart shows the ratio of cell viability between *MUS81*$^{-/-}$ *DNPH1*$^{-/-}$ vs *MUS81*$^{-/-}$ (mean with s.e.m; n=3).

(E) DLD1 WT or KO cell lines were treated for 10 days with olaparib in the absence or presence of hmdU (50 nM). Cell viability was determined as in (B). *BRCA2*$^{-/-}$ *DNPH1*$^{-/-}$ vs *BRCA2*$^{-/-}$ *DNPH1*$^{-/-}$ + hmdU, $p < 0.0001$. DLD1 WT and *BRCA2*$^{-/-}$ cells treated with olaparib only are from (C).

Europe PMC Funders Author Manuscripts

Europe PMC Funders Author Manuscripts

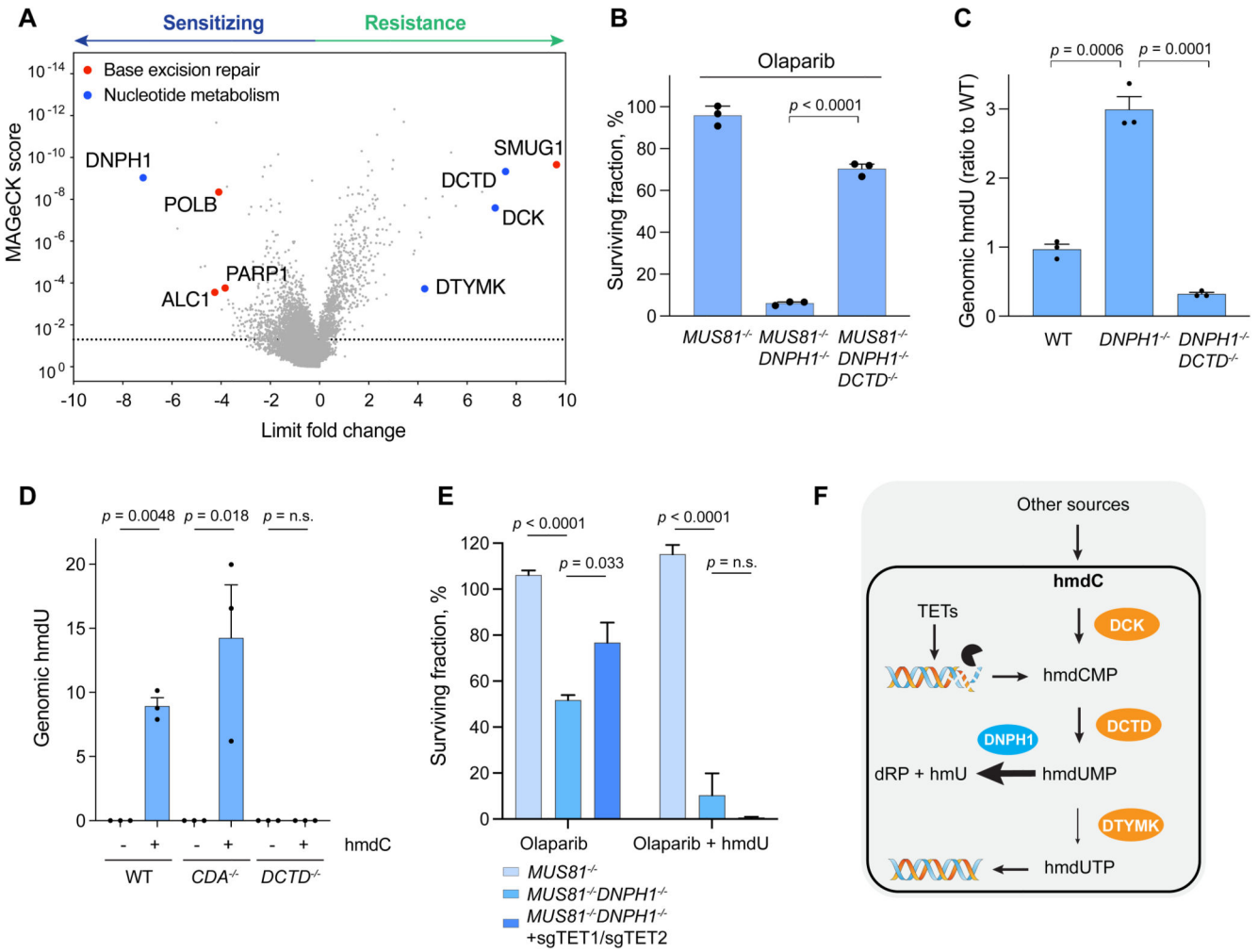

Fig. 4. hmdU is produced by metabolism of epigenetically modified nucleotides.

(A) Volcano plot showing sgRNA scores from MAGeCK analysis of CRISPR-Cas9 hmdC dropout/enrichment screen. Data are represented as in Fig. 1A (n=3).

(B) eHAP KO cell lines were continuously treated with olaparib (50 nM) for 6 days and cell viabilities were determined using CellTiter-Glo.

(C) Genomic DNA was extracted from the indicated eHAP cell lines, digested, and analyzed for hmdU by LC-MS. The ratio of hmdU levels to WT is indicated (mean with s.e.m; n=3).

(D) eHAP cell lines were treated with hmdC (0.2 μM) for 24 hours. Genomic DNA was extracted, digested, and analyzed for hmdU by LC-MS. The relative genomic hmdU levels are indicated (mean with s.e.m; n=3)

(E) eHAP *MUS81*$^{-/-}$, *MUS81*$^{-/-}$ *DNPH1*$^{-/-}$ or *MUS81*$^{-/-}$ *DNPH1*$^{-/-}$ cells transduced with lentiCRISPR-sgTET1 and sgTET2 were treated with olaparib (25 nM) in the absence or presence of hmdU (50 nM) for 6 days. Cell viability was determined as in (B).

(F) Schematic showing the metabolism of hmdC originating from TET-mediated hydroxymethylated cytosine and other extracellular sources. Breakdown of DNA (for example, during DNA repair) releases epigenetically marked nucleotides, such as hmdCMP. To prevent their re-incorporation, they are degraded in a two-step process; (i) hmdCMP is

deaminated to cytotoxic hmdUMP by DCTD, and (ii) DNPH1 hydrolyzes hmdUMP into hmU and dRP. DNPH1 deficiency leads to excess hmdUMP that becomes phosphorylated to hmdUTP by DTYMK and incorporated in DNA.

Europe PMC Funders Author Manuscripts

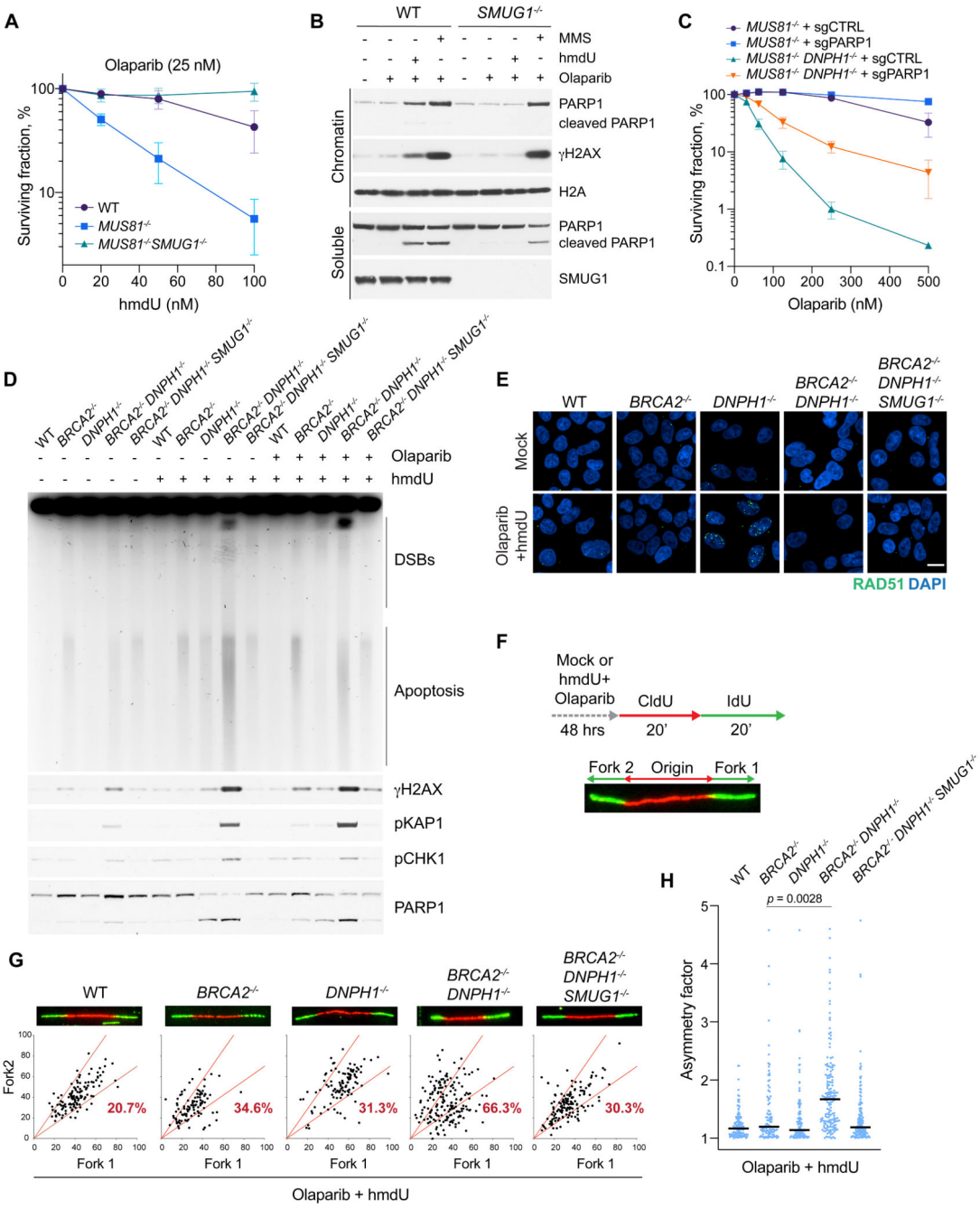

Fig. 5. hmdU promotes PARP trapping, DSB formation, and cell death through the actions of SMUG1.

(A) eHAP WT and KO cell lines were treated with olaparib (25 nM) and the indicated doses of hmdU for 6 days. Cell viability was determined using CellTiter-Glo (n=3). *MUS81*$^{-/-}$ vs *MUS81*$^{-/-}$ *SMUG1*$^{-/-}$, $p = 0.0014$.

(B) eHAP WT and *SMUG1*$^{-/-}$ cells were either untreated or pre-treated for 24 hours with hmdU (0.35 μM) or 2 hours with MMS (0.01%) followed by olaparib (10 μM) for 4 hours. Following subcellular fractionation the nuclear soluble or chromatin fractions were analyzed by immunoblotting with the indicated antibodies.

(C) eHAP *MUS81*$^{-/-}$ or *MUS81*$^{-/-}$ *DNPH1*$^{-/-}$ cells were transduced with lentiCRISPR-sgPARP1 or control (sgCTRL) and treated with olaparib for 6 days. Cell viability was determined as in (A). *MUS81*$^{-/-}$ *DNPH1*$^{-/-}$*/sgCTRL* vs *MUS81*$^{-/-}$ *DNPH1*$^{-/-}$/sgPARP1, $p < 0.0001$.

(D) Top: PFGE analysis of DNA break formation in DLD1 WT or KO cell lines either untreated or treated with hmdU (2 μM) or co-treated with olaparib (0.1 μM) and hmdU (100 nM) for 72 hours. DNA breaks were visualized by ethidium bromide staining. Bottom: the same samples were analyzed by immunoblotting.

(E) DLD1 WT and KO cell lines were either untreated or treated with olaparib (10 nM) and hmdU (0.1 μM) for 48 hours and subjected to immunofluorescence staining with a RAD51 antibody (green). DNA was stained by DAPI (blue). Scale bar is 10 μm.

(F) Schematic overview of DNA fiber analysis. DLD1 WT or KO cells were untreated or co-treated with olaparib and hmdU for 48 hrs. Cells were labeled with CldU (20 mins; 20 μM) followed by IdU (20 mins; 150 μM). DNA fibers were spread on glass slides and subjected to immunofluorescence staining with CldU (red) and IdU (green) antibodies. Fork symmetry was assessed by measuring the lengths of the two bidirectional forks.

(G) Plots showing the lengths of the bidirectional forks in DLD1 cell lines treated with olaparib (0.1 μM) and hmdU (1 μM) for 48 hrs. Bidirectional forks with >30% difference in lengths (outside red lines) were scored as asymmetrical and shown as percentage.

(H) Plots showing the asymmetry factor from forks in (G). Horizontal line represents the median. *BRCA2*$^{-/-}$ vs *BRCA2*$^{-/-}$ *DNPH1*$^{-/-}$, $p = 0.0028$.

Europe PMC Funders Author Manuscripts

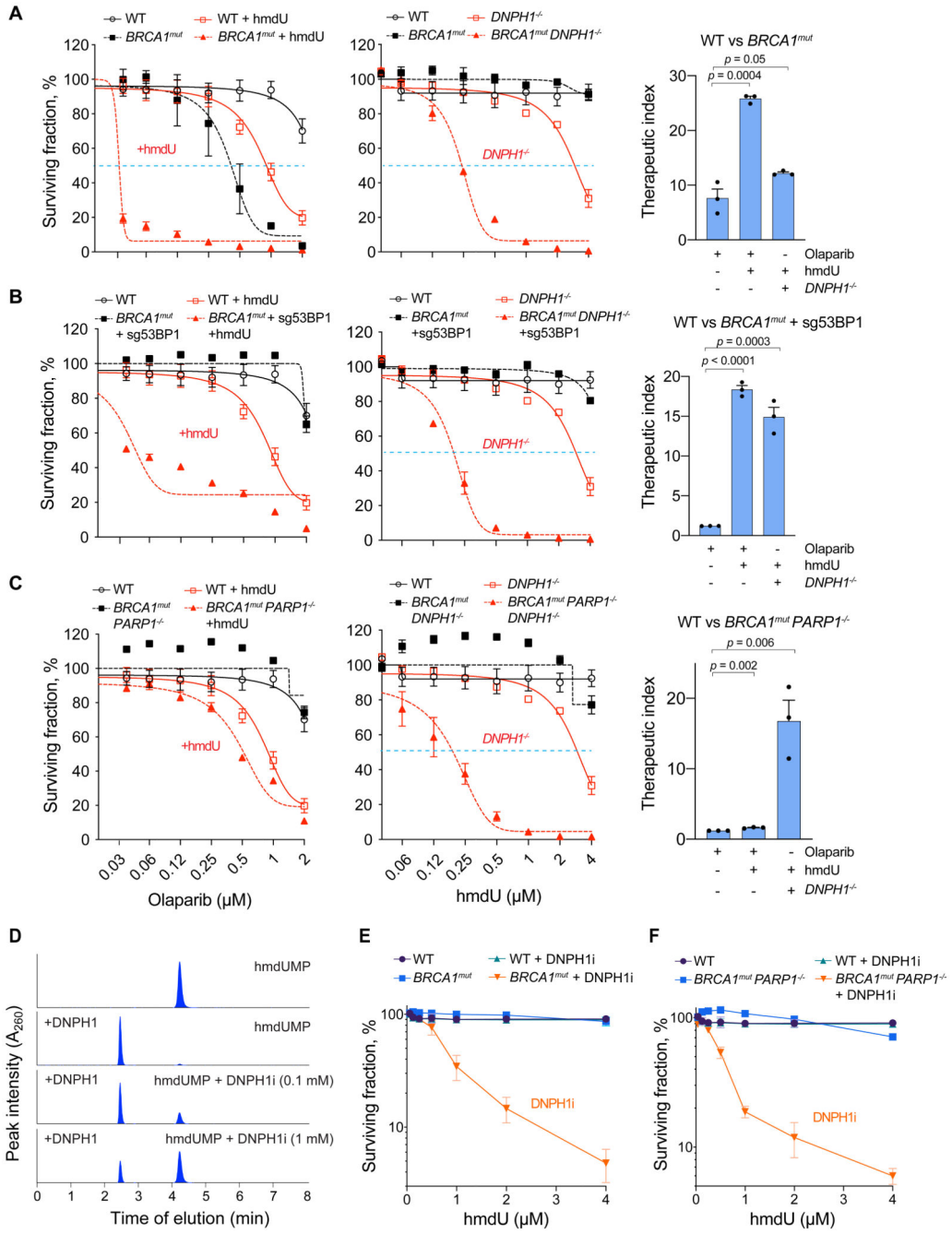

Fig. 6. Killing of PARPi-resistant *BRCA1* cells by targeting DNPH1.

(A) Left panel: SUM149 *BRCA1*^{mut} (parental) and WT (revertant) cell lines were either untreated or treated with olaparib in the absence (black lines) or presence of hmdU (2 μM; red lines) for 8 days. Cell viability was determined using CellTiter-Glo (mean with s.e.m; n=3). Blue dotted line represents EC50 values. Center panel: As (left) but SUM149 *BRCA1*^{mut} (parental) and WT cell lines were either untreated or treated with the indicated doses of hmdU in the absence (black lines) or presence of *DNPH1* KO (red lines) for 8 days.

Right panel: Therapeutic index of the indicated treatments calculated from the ratio of EC50 values from (left) and (center) in SUM149 WT vs. *BRCA1*^{mut} cells.

(B) Left: SUM149 *BRCA1*^{mut}/sg53BP1 or WT (revertant) cell lines were treated as in (A, left). For direct comparison, curves of WT and WT + hmdU from (A, left) are shown (solid black and red lines, respectively). Center: SUM149 *BRCA1*^{mut}/sg53BP1 or WT cell lines were treated as in (A, center). For direct comparison, curves of WT and *DNPH1*$^{-/-}$ from (A, center) are shown (solid black and red lines, respectively). Right: Therapeutic index of the indicated treatments calculated from the ratio of EC50 values from (left) and (center) in SUM149 *BRCA1*^{mut}/sg53BP1 cells.

(C) Left: SUM149 *BRCA1*^{mut} *PARP1*$^{-/-}$ or WT cell lines were treated as in (A, left). For direct comparison, curves of WT and WT + hmdU from (A, left) are shown (solid black and red lines, respectively). Center: SUM149 *BRCA1*^{mut} *PARP1*$^{-/-}$ or WT cell lines were treated as in (A, center). For direct comparison, curves of WT and *DNPH1*$^{-/-}$ from (A, center) are shown (solid black and red lines, respectively). Right: Therapeutic index of the indicated treatments calculated from the ratio of EC50 values from (left) and (center) in *BRCA1*^{mut} *PARP1*$^{-/-}$ cells.

(D) Inhibition of DNPH1 activity towards hmdUMP by N6-benzyl-AMP (DNPH1i). DNPH1 (4 μM) was incubated with hmdUMP (1 mM) in the absence or presence of DNPH1i for 45 min. Products were analyzed by RP-HPLC and visualized as chromatograms.

(E) SUM149 *BRCA1*^{mut} (parental) and WT (revertant) cell lines were either untreated or treated with hmdU in the absence or presence of DNPH1i (0.3 μM) for 8 days. Viability was determined using CellTiter-Glo (mean with s.e.m; n=3). *BRCA1*^{mut} vs *BRCA1*^{mut} + DNPH1i, $p < 0.0001$.

(F) SUM149 *BRCA1*^{mut} *PARP1*$^{-/-}$ or WT (revertant) cell lines were treated as in (E) (mean with s.e.m; n=3). *BRCA1*^{mut} *PARP1*$^{-/-}$ vs *BRCA1*^{mut} *PARP1*$^{-/-}$ + DNPH1i, $p < 0.0001$.